Functional Inertia Index of Memory-Retaining Brain Dynamics: A Measure of Large-Scale Brain Adaptability

Sir-Lord Wiafe[1], Vince D. Calhoun[1]

[1]Tri-Institutional Center for Translational Research in Neuroimaging and Data Science (TReNDS), Georgia State University, Georgia Institute of Technology, and Emory University, Atlanta, GA 30303, USA.

Abstract

Adaptive cognition relies on brain activity that is both flexible and resilient to noise, a property we term functional inertia. Conventional dynamic fMRI metrics treat networks as memoryless and cannot capture the persistence that makes some states fleeting and others entrenched. We introduce the functional inertia index (FII), the first index to quantify temporal momentum by measuring the force required to deviate from a brain's long-running trajectory. Applied to resting-state fMRI from a multisite schizophrenia cohort, FII revealed distinct recurrent states, with prolonged residence in a high-inertia plateau predicting greater symptom severity. This effect was mediated by whole-brain FII, which also showed a positive relationship with cognition in patients but a negative relationship in controls, revealing a dissociation between adaptive and maladaptive rigidity. At the regional level, FII unifies two long-standing observations in schizophrenia: excessive rigidity in associative hubs and pathological volatility in sensory pathways, situating both within a single inertial framework and offering a candidate dynamic biomarker.

Keywords: Functional Inertia Index (FII), neural adaptability, fMRI, Schizophrenia, dynamic time warping.

1. INTRODUCTION

Neural population activity is often depicted as a carousel of fleeting network states: primary visual cortex can reverse its coupling polarity within a few hundred milliseconds, whereas association cortex integrates information across several seconds [1,2]. Yet each fluctuation inherits momentum from what came before. Recurrent excitation [3], synaptic N-methyl-D-aspartate (NMDA) currents [4], and the slow summation of the blood oxygenation level-dependent (BOLD) response [5] endow cortical circuits with a "memory," conferring **functional inertia**, i.e., an established dynamical pattern will persist unless the incoming drive is exceptionally strong or prolonged. Here, for the first time, we directly and quantitatively operationalized functional inertia across whole-brain dynamics.

Most dynamic functional magnetic resonance imaging (fMRI) techniques, such as sliding window correlations, instantaneous phase synchronization, instantaneous co-activation patterns, dynamic gradient approaches, and dynamic independent primitives [6-10], treat the network as memoryless: each window forgets anything older than its span. This misses the temporal momentum that makes some states fleeting and others resistant. That gap is critical. Adaptive cognition requires the brain to reorganize efficiently when needed, but also to resist transient noise. When inertia is mistuned, networks may become either excessively rigid or pathologically volatile. Indeed, prior work has described a kind of "functional inertia" in the brain—such as lingering co-activation patterns after emotional events [11], prolonged dwell times in maladaptive connectivity states [12,13], and rigidity of internal models in hypoplastic computational regimes [14]. These observations establish that inertia-like phenomena exist in brain dynamics, but a unified, tractable index has remained absent, leaving functional inertia as an unmeasured but clinically important construct.

Here we introduce the functional inertia index (FII), a cumulative-window dynamic time warping (DTW) framework that operationalizes this property by quantifying, frame by frame, the force required to deviate from the brain's long-running amplitude trajectory. DTW provides a time-normalization framework between two sequences [15], enabling amplitude-discrepancy trajectories to be quantified without confounds from differing timescales [16,17], a property particularly relevant for brain processes [1]. By accumulating DTW distances and taking their derivative, the FII captures this deviation force directly, transforming the abstract notion of functional inertia into a measurable property of brain dynamics. Importantly, higher FII values indicate greater deviation force and therefore lower inertia (greater adaptability), whereas values near zero indicate higher inertia (rigidity), where fluctuations are absorbed into the ongoing configuration.

We explore the single question: *"Does dysregulated functional inertia—over-rigid in core networks, over-volatile in sensory bridges—explain why schizophrenia locks the brain into maladaptive states while healthy brains exploit inertia to stabilize efficient ones?"* Two lines of prior evidence make this question pressing. First, dynamic functional connectivity studies show that patients linger in hypoconnected or weakly integrated states that scale with symptom severity [12,18]. Second, computational work demonstrates

that excessive cortical attractor stability or, conversely, noisy thalamo-sensory loops can produce hallucinations and cognitive rigidity [19,20]. Together, these findings suggest that mistuned inertia may weld the system into maladaptive configurations while allowing pathological volatility elsewhere.

To build intuition for what functional inertia captures, it is useful to borrow language from classical mechanics. Imagine each large-scale circuit as a weighted spring. When an external drive arrives, a flexible spring (low inertia) recoils almost instantly, whereas a rigid spring (high inertia) hardly moves unless the force is sustained. In the brain, BOLD-indexed amplitude distance is the instantaneous "displacement," and the derivative of the cumulative trajectory, the FII, represents the force required to alter that displacement against the spring's mass. A near-zero FII indicates high inertia, where incoming fluctuations are absorbed with little effect, while a large positive or negative FII indicates lower inertia, where sufficient force is applied to overcome stored momentum and reconfigure large-scale dynamics. In a healthy brain, this inertia may act as ballast by filtering out transient noise while preserving coherent activity [21,22], and may grant higher-order associative networks the continuity needed for sustained cognition [23]. Our working hypothesis is that the schizophrenia brain mis-calibrates this hierarchy, rendering core networks excessively inert and certain sensory-integration pathways excessively labile, thereby locking maladaptive patterns in place while allowing disruptive volatility elsewhere. Although we test this hypothesis in schizophrenia, the framework generalizes to any condition where brain stability and adaptability are disrupted, and the principle of deriving inertia from cumulative dynamics can be implemented with metrics beyond DTW, making the approach broadly extensible.

Applying the FII to a multi-site cohort (160 controls and 151 individuals with schizophrenia), our framework unifies three cardinal observations: (i) it accounts for the opposite occupancy of high- versus low-inertia states in schizophrenia and health, (ii) it predicts and mechanistically explains why whole-brain FII scales with clinical symptoms, mediates the impact of prolonged time in high-inertia plateaus, and relates in opposite directions to cognition across groups, and (iii) at the network level, it reconciles two long-standing observations in schizophrenia by showing that associative hubs are pathologically rigid while sensory pathways are pathologically volatile, situating both abnormalities within a single framework. Taken together, these findings establish the first tractable index of memory-retaining brain dynamics, offering a general framework for quantifying adaptability and rigidity in health and disease and positioning FII as a candidate dynamic biomarker that unifies group differences, cognition, and symptom burden.

2. RESULTS

2.1. Functional inertia states and clinical relevance

We applied k-means clustering to functional inertia index trajectories, defined as the derivative of the cumulative DTW profiles, from both individuals with schizophrenia and healthy controls to identify recurring states in the brain's temporal amplitude dynamics. Because FII is the derivative of the cumulative DTW, larger values indicate lower inertia

(greater adaptability) while near-zero values indicate high inertia (rigidity). For interpretability, we sign-flipped FII so that positive values correspond to a stabilizing trajectory with decreasing amplitude disparity, and negative values correspond to a shifting trajectory with increasing disparity relative to the long-running configuration. The clustering revealed three distinct states (Fig. 1a,b): state 1, stabilizing (amplitude disparities diminish over time), state 2, locked (derivatives near zero; high inertia; resistance to deviation), and state 3, shifting (amplitude disparities increase over time). We use these labels henceforth. In keeping with the spring analogy, high inertia reflects rigidity that resists change, whereas low inertia reflects flexibility that enables adaptation.

Group comparisons of state engagement revealed that patients spent significantly more time in the stabilizing state and less time in the locked state than controls, as indexed by both FR and MDT (Fig. 1c-d; *purple asterisk*). Conversely, controls exhibited significantly greater engagement with the locked state than patients (Fig. 1c-d; *green asterisk*). No significant group differences were observed in the transition probabilities across states.

We next examined associations between state metrics and clinical or cognitive profiles, as assessed by PANSS and CMINDS, respectively. State metrics showed significant associations with symptom severity but not with cognitive performance. Higher positive and negative symptom scores were associated with greater persistence within the locked state, reflected through increased self-transitions and reduced transitions from the locked state to other states (Fig. 1f, h). Additionally, positive symptom severity was positively associated with both FR and MDT in the locked state and negatively correlated with the FR of the shifting state (Fig. 1g). A similar pattern was observed for negative symptoms, which were associated with increased FR in the locked state and decreased MDT and FR in the shifting state (Fig. 1i).

First, individuals with schizophrenia spend more time in the stabilizing state and less time in the locked state than controls. Second, within patients, greater engagement with the locked state across FR, MDT, and self-transitions consistently tracks higher positive and negative symptom severity, while reduced engagement with the shifting state relates to greater burden, especially for negative symptoms. These associations show that FII captures clinically relevant rigidity and volatility beyond conventional dynamic metrics.

Fig. 1: FII states & clinical relevance

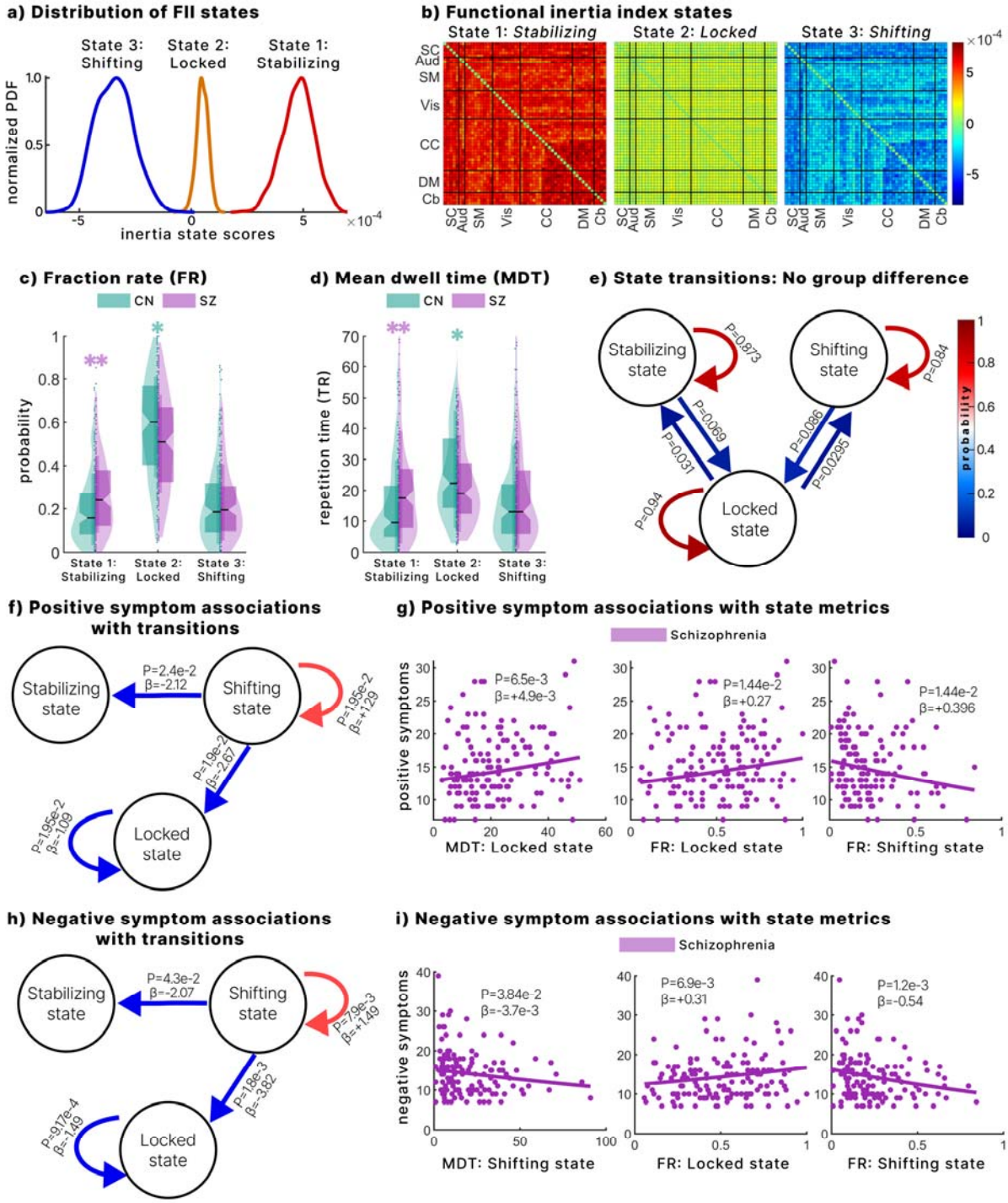

(a) Empirical distribution of the three FII states after sign-flipping: the stabilizing state (positive derivatives), the locked state (near-zero derivatives, high inertia), and the shifting state (negative derivatives). (b) State matrices. (c) fractional rate (FR) and (d) mean dwell time (MDT) for each state in healthy controls (CN) and patients with schizophrenia (SZ); asterisks show significance ($\alpha = 0.05$). (e) Group-averaged state-to-state transition probabilities. Associations between positive symptoms and (f) probability transitions and (g) state metric (MDT, FR). Parallel associations for negative symptoms are illustrated in (h) and (i). All effects were estimated with generalized linear models controlling for sex, age, site, and mean framewise displacement; p-values were false-discovery-rate corrected (p < 0.05). Significance keys: $(*)\ 0.05 > p \geq 0.01$; (**) $0.01 > p \geq 0.001$; (***) $p < 0.001$.

2.2. Global FII and cognition

To test whether clinical burden relates to whole-brain flexibility, we examined associations between global FII (the mean absolute FII across time) and PANSS and CMINDS scores, separately for patients and controls. By construction**,** higher global FII indicates lower inertia (greater adaptability), whereas lower values indicate higher inertia (reduced adaptability). Among individuals with schizophrenia, the global FII showed significant negative associations with both positive and negative PANSS scores (Fig. 2a), indicating that higher overall derivative values (i.e., lower inertia or greater neural adaptability) were linked to lower symptom severity. Furthermore, the global FII was positively associated with processing speed scores, indicating that a higher global FII is linked to increased processing speed. In contrast, controls showed an inverse pattern: global FII was negatively associated with processing speed, working memory, verbal and visual learning, reasoning and problem-solving, and the CMINDS composite cognitive score (Fig. 2b). These findings indicate that in schizophrenia, higher global FII (greater adaptability, lower inertia) relates to lower symptom severity and better processing speed, whereas in controls, lower global FII (greater inertia) relates to better performance across multiple cognitive domains. These opposite associations underscore that FII captures dimensions of network stability and adaptability not detected by conventional dynamic metrics.

Fig. 2: Global FII and cognition

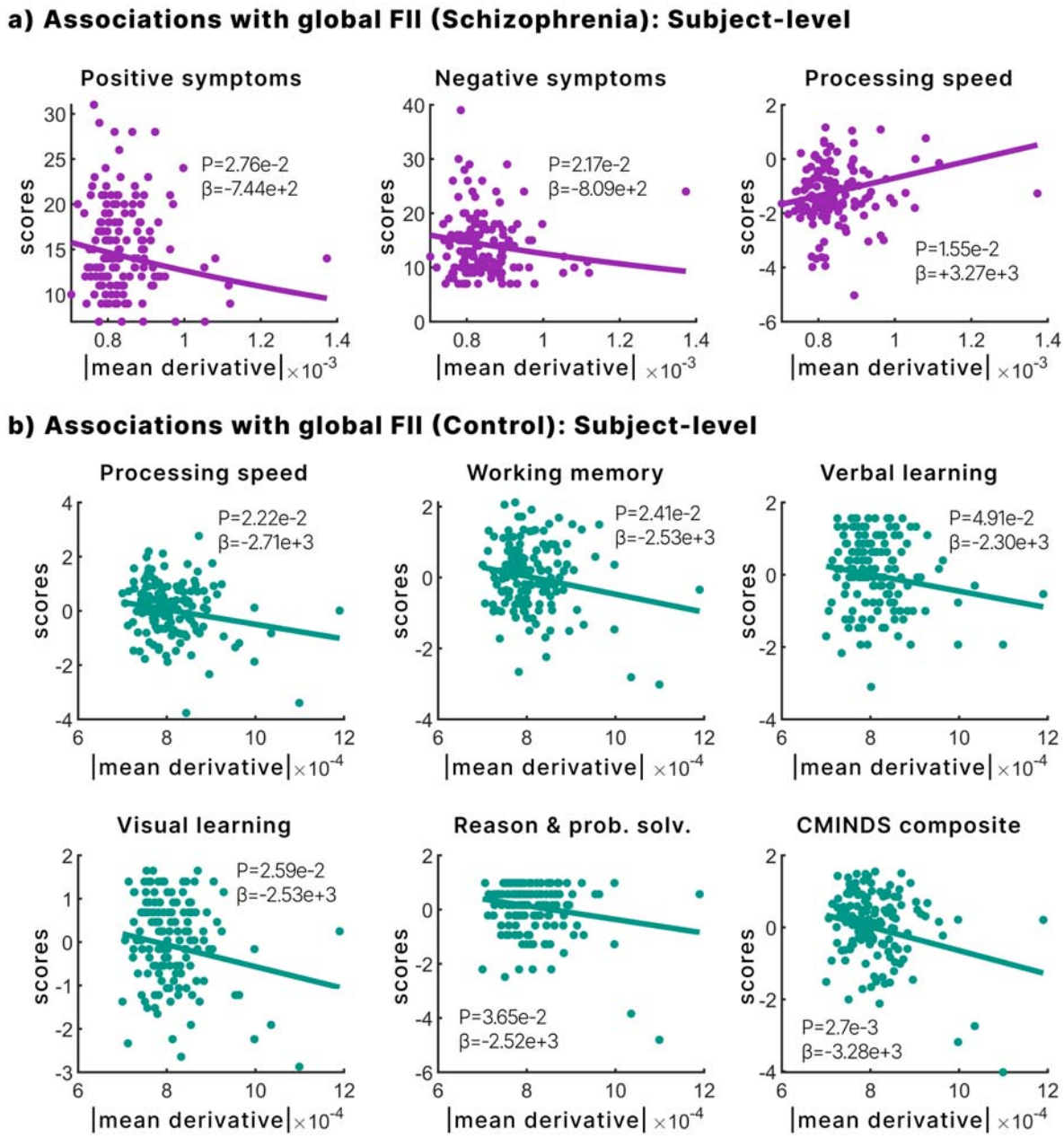

Global FII, defined as the mean absolute derivative of the cumulative DTW trajectory across all network pairs, provides one value per participant. (a) In schizophrenia (SZ), higher global FII (greater adaptability, lower inertia) was associated with lower PANSS positive and negative scores and with faster processing speed. (b) In healthy controls (CN), lower global FII (greater inertia) was associated with better performance across processing speed, working memory, verbal and visual learning, reasoning and problem-solving, and the CMINDS composite cognitive score.

2.3. Network-resolved FII analysis

To localize the associations observed at the global level, we examined relationships between FII across our 1,378 unique brain region pairs and both symptom severity and cognitive performance. For positive symptoms, 12 functional connections were significantly associated with PANSS-positive scores after FDR correction (Fig. 3a). Of these, 10 edges (83%) showed negative regression coefficients, indicating that higher FII (lower functional inertia and greater adaptability) was associated with lower symptom severity. These negatively associated connections spanned a broad set of circuits, including midline default-mode network hubs (e.g., posterior cingulate cortex), limbic–thalamo–temporal pathways, and fronto-striatal as well as cerebellar links.

Two connections showed the opposite effect, with positive regression coefficients, where higher FII (lower functional inertia and greater adaptability) was associated with higher positive symptom severity. These edges linked primary sensory cortices, including somatosensory and visual areas, to higher-order association hubs, specifically the posterior cingulate cortex (PCC) and inferior parietal lobule (IPL), suggesting a distinct subset of sensorimotor–default-mode and visuo-parietal pathways showing divergent behavior.

For negative symptoms, 29 region pairs were significantly associated with PANSS-negative scores (Fig. 3a). Among these, 24 edges (also 83%) exhibited negative regression coefficients, again indicating that higher adaptability was associated with lower negative symptom severity. These edges involved several functional systems, including midline default-mode regions (ACC, PCC, precuneus), temporal-sensorimotor connections (e.g., fusiform and superior temporal gyri coupled with the postcentral gyrus), and occipito-parietal–sensorimotor interactions (e.g., cuneus and superior parietal lobule connected to the postcentral cortex and cerebellum).

The remaining five edges for negative symptoms showed positive associations, where greater adaptability corresponded to greater symptom severity. These connections were primarily located in parietal and occipital association areas, including the bilateral inferior parietal lobule, paracentral lobule, calcarine cortex, and middle occipital gyrus, with links either within these regions or to the ACC.

Across both positive and negative symptoms, most brain connections followed the global rule: higher global FII related to lower symptom severity. A subset of edges, particularly those linking sensorimotor with association regions for positive symptoms and parietal–occipital regions for negative symptoms, showed the opposite effect, suggesting region-specific deviations. In line with the spring analogy, most circuits behave as expected, where greater flexibility (lower inertia) alleviates burden, yet a minority resists this pattern, underscoring region-specific tensions between stability and adaptability. Together, these results point to schizophrenia as a disorder of a rigid associative core and a volatile sensory periphery, unified by a common inertial mechanism.

Fig. 3: Network-resolved FII analysis.

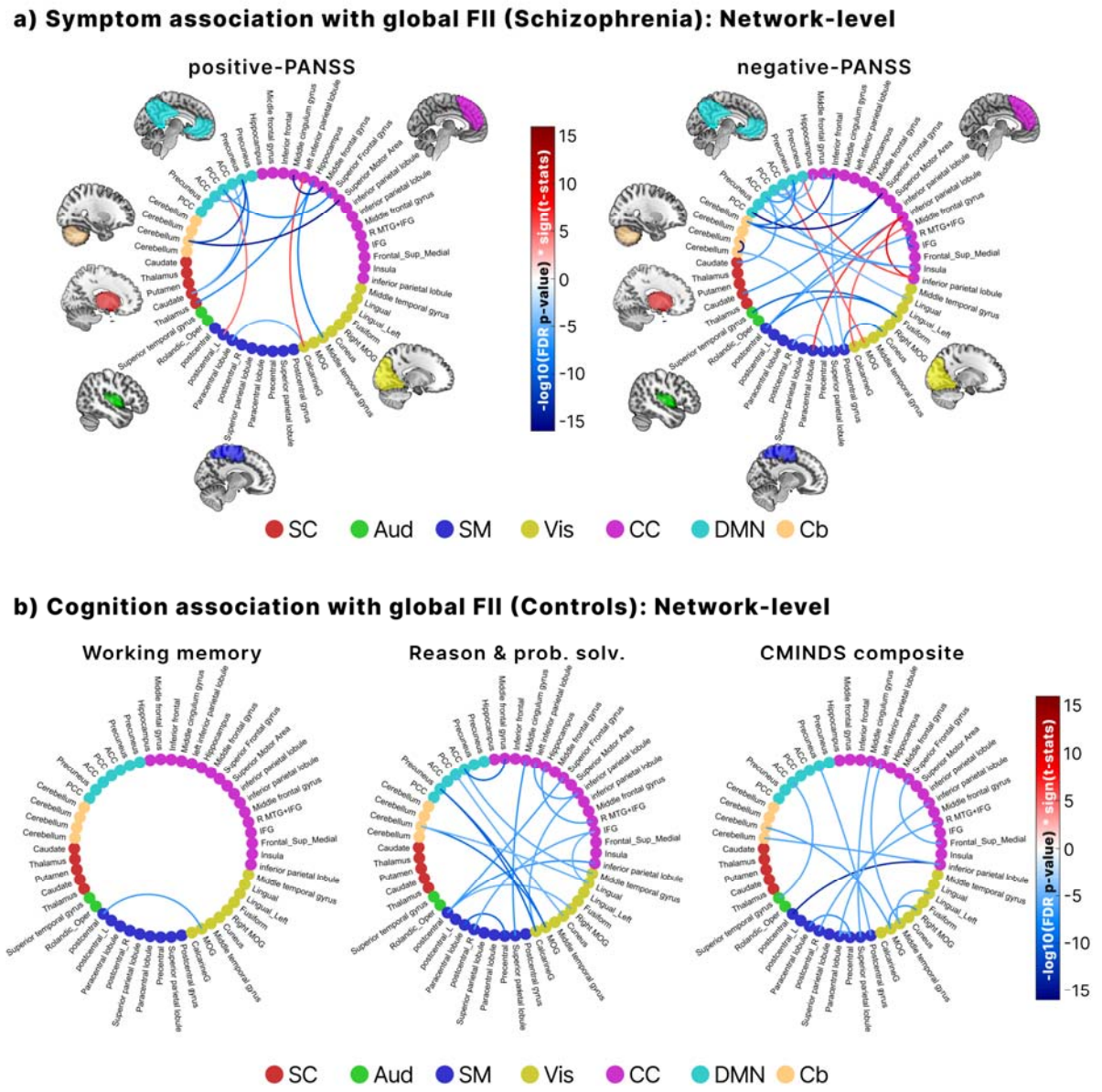

Network-specific adaptability was quantified as the mean absolute FII, computed for every pair of intrinsic brain networks. (a) Schizophrenia cohort: Most implicated edges linked default-mode, limbic–thalamic, and fronto-striatal pathways, where greater FII (lower inertia) related to lower symptom burden, consistent with core schizophrenia circuits. A minority of sensorimotor–visual to association edges showed the opposite effect, aligning with reports of perceptual instability. (b) In controls, significant edges primarily involved default-mode and fronto-parietal networks, where greater FII predicted better cognitive performance, in line with their roles in executive function.

Red edges denote a significant positive association; blue edges denote a significant negative association. All GLMs control for age, sex, acquisition site, and mean framewise displacement. Only connections surviving FDR correction ($p < 0.05$, $\alpha = 0.05$) are displayed.

2.4. Mediation analysis

We next tested whether the relationship between prolonged engagement in the locked state and clinical symptom severity operates through the brain's global inertia, operationalized through the global FII. This was evaluated through a mediation framework, and all three conditions for statistical mediation were met.

First, the a-path was significant: across schizophrenia patients, greater engagement with the locked state predicted lower global FII. Specifically, the global FII was negatively associated with the locked state's fraction rate, mean dwell time, and self-transition probability ($\beta = -4.59 \times 10^{-2}\ to - 9.42 \times 10^{-4},\ p < 10^{-8}$; Fig. 4a). Second, the b-path was satisfied: lower global FII predicted higher symptom severity, even after accounting for the locked state engagement. When both the global FII and the relevant locked state metric (fraction rate for both symptom domains, mean dwell time for positive symptoms) were included in the same model, the global FII maintained significant negative associations with both PANSS-positive and PANSS-negative scores ($\beta = -1.27 \times 10^{3}\ to\ - 0.11 \times 10^{3}, \mathrm{p} < 0.03$; Fig. 4b). Third, inclusion of the global FII in the model reduced the previously significant associations between the locked state metrics and symptom severity to non-significance, indicating that the c′-path, the direct relationship between the locked state engagement and symptoms, was no longer present after accounting for global FII (Fig. 4c).

A bias-corrected bootstrap test using 5,000 resamples confirmed significant indirect effects. For positive symptoms, the mediated effect through the locked state's fraction rate yielded an indirect path coefficient $a \times b = 0.32\ (95\ \%\ CI: 0.06 - 0.58;\ p = 9.9 \times$ *10−3*, and through the locked state's dwell time, *a × b = 4.3×10−3 95 % CI: 0.8×10−3−7.9×10−3; p = 8.8×10−3*. For negative symptoms, the indirect effect via the locked state's fraction rate was $a \times b = 0.24\ (95\ \%\ CI: 0.03 - 0.45;\ p = 1.39 \times 10^{-2})$. All confidence intervals excluded zero, indicating statistically significant mediation.

These findings confirm that global FII mediates the link between locked-state engagement and symptom burden (consistent with the inversion: lower global FII = higher inertia = worse symptoms), moving beyond correlation and adding mechanistic plausibility. Together with the state and global analyses, this positions FII as a candidate dynamic biomarker that unifies group differences, cognition, and symptom severity, while capturing memory-retaining properties of brain dynamics beyond conventional metrics.

Fig. 4: Mediation analysis

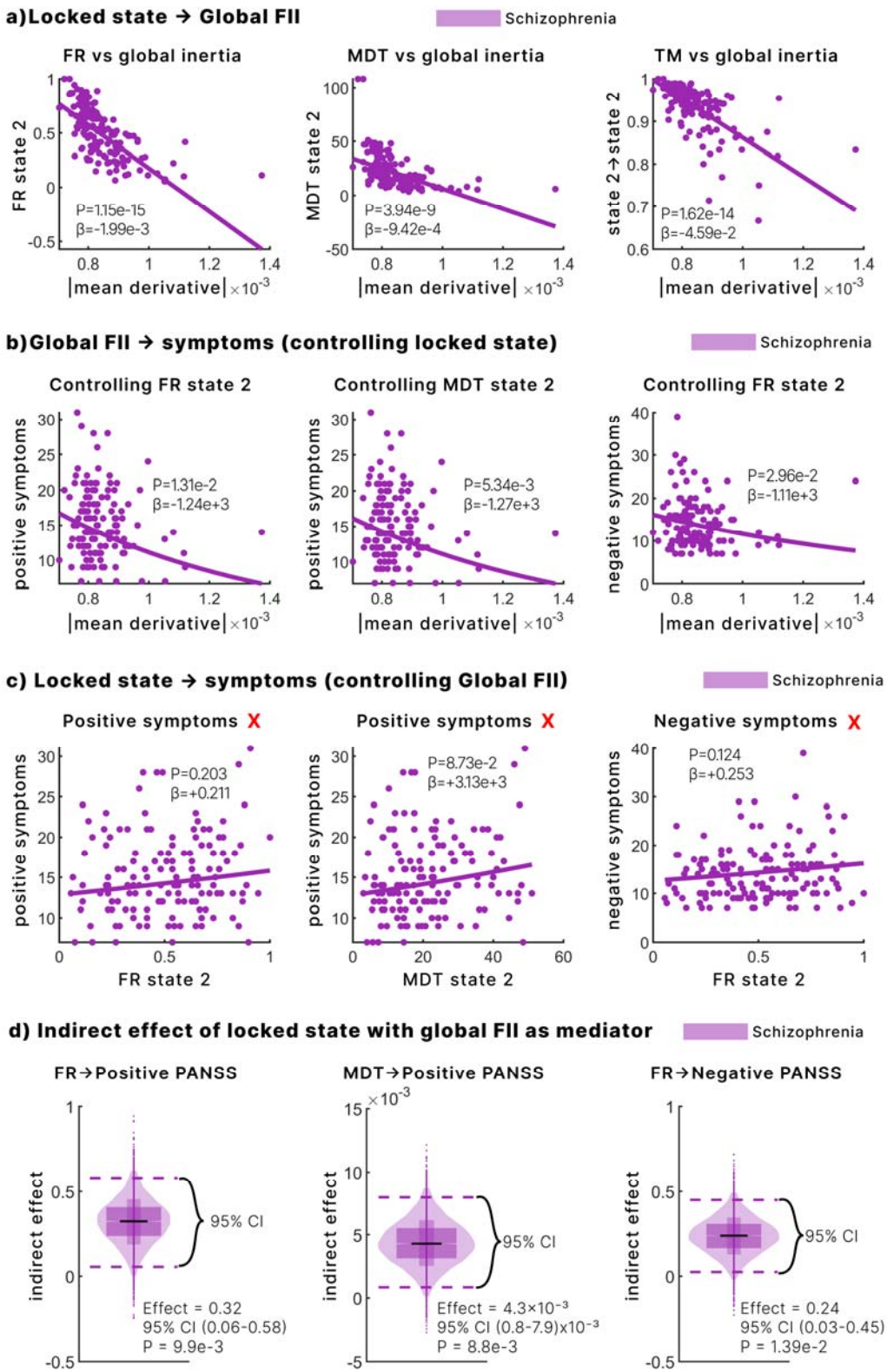

(a) State dynamic metrics (MDT, FR, TM) association with global FII (a-path). (b) association between global FII and symptoms while controlling for state 2 dynamic metrics (b-path). (c) association between state 2 dynamic metrics and symptoms while controlling for global FII (c'-path). Red crosses indicate no significance ($\alpha = 0.05$). (d) Indirect effect. Bootstrap sampling distribution (5,000 resamples) of the product $a \times b$; dashed horizontal lines show the 95 % percentile confidence interval. Mediation is significant because the interval excludes zero.

3. DISCUSSION

This Brain dynamics are commonly described as a stream of moment-to-moment network flashes, yet every fluctuation carries the momentum of its immediate past [24,25]. Here, we provide, to our knowledge, the first metric that directly quantifies that momentum by measuring the force a new network pattern must exert to rewrite its running functional configuration. The method extends our recently developed time-resolved dynamic time warping framework [17], which aligns regional BOLD-amplitude trajectories. By adding a cumulative-window computation, we obtain a data-driven measure of functional inertia that estimates how strongly preceding network states constrain subsequent reconfigurations. This captures the memory-retaining properties of brain dynamics that conventional dynamic metrics overlook.

Clustering the inertia trajectories uncovered three recurring network states (Fig. 1a, b). The stabilizing state showed uniformly positive derivatives, marking periods when inter-regional amplitude disparities were diminishing. The shifting state displayed uniformly negative derivatives, indicating widening disparities. Interposed between them, the locked state was centered near zero derivatives, a high-inertia plateau in which the current functional configuration resisted change. Relative to controls, patients spent significantly more time and had longer dwell times in the stabilizing state (diminishing disparities, but not necessarily healthy stabilization), but markedly less time in the locked state; controls, by contrast, preferentially occupied the high-inertia plateau (Fig. 1c, d).

Reduced occupancy of the high-inertia locked state might appear to suggest greater lability, but schizophrenia does not begin from a balanced baseline. Converging evidence from PET and fMRI work together with our own earlier DTW study shows that the disorder is marked by enduring, spatially nonuniform functional dynamics [17,26,27]. In that context, the experience of a high-inertia state for patients represents a pathological steady state: when the system settles there, its aberrant configuration is effectively locked in. Consistent with this view, the patients who lingered longest in the locked state were precisely those with the highest positive and negative PANSS scores (Fig. 1f–i). Thus, the liability in schizophrenia is not heightened flexibility but the tendency to remain stuck in a low-adaptability, high-inertia regime that preserves an already pathological distribution of activity. In keeping with our spring analogy, schizophrenia is marked not by healthy resistance but by pathological rigidity, where the system's ballast holds it in maladaptive configurations. Echoing dynamic-connectivity studies in which

prolonged residence in hypoconnected or weakly integrated states predicts greater symptom burden [12,18], our results extend this persistence motif by showing that the rigidity associated with symptom severity emerges most clearly when the brain enters the high-inertia state captured for the first time with cumulative-window DTW. This establishes our first cardinal insight: schizophrenia and health show opposite occupancy of high- versus low-inertia states, a contrast that at first glance suggests greater flexibility in patients but in fact reflects pathological rigidity, as symptom severity rises with prolonged locked-state engagement.

Whole-brain analyses supported this dissociation. In patients, higher values of the global FII, indicating lower whole-brain inertia, were associated with lower PANSS positive and negative scores and with faster processing-speed performance (Fig. 2a). Mediation analysis further demonstrated that global FII mechanistically links prolonged locked-state engagement to symptom burden, underscoring its role as more than a correlational index (Fig. 4). Thus, individuals who can deviate more forcefully from entrenched network patterns appear to attain better clinical outcomes, echoing behavioral evidence of cognitive rigidity in schizophrenia, such as perseverative errors and set-shifting deficits [28], and aligns with longitudinal work showing that antipsychotic treatment increases connectivity variability in default mode and control circuits as symptoms abate [29]. In controls, the pattern reversed: lower global FII (higher inertia) correlated with superior performance across multiple CMINDS domains, including verbal and visual learning, working memory, reasoning/problem solving, processing speed, and the composite cognitive index (Fig. 2b). This mirrors evidence that greater connectome stability tracks better cognitive performance in neurotypical cohorts [30].

Taken together, these findings reinforce a principled view: high functional inertia is advantageous when the system occupies a balanced and well-regulated baseline but becomes detrimental when the baseline configuration is already abnormal, as in schizophrenia, with mediation analysis confirming that whole-brain FII provides the mechanistic bridge linking prolonged locked-state engagement to symptom burden. This constitutes our second cardinal observation, highlighting global FII as a unifying, mechanistic marker of adaptability versus rigidity.

At the circuit level, the relation between functional inertia and symptom severity was both widespread and anatomically selective. Approximately 83% of edges that survived FDR correction followed a consistent rule: larger amplitude derivatives, reflecting lower functional inertia, predicted lower PANSS scores (Fig. 3a). For positive symptoms, edges showing inverse symptom relations linked midline default-mode network hubs such as the posterior cingulate cortex with limbic, thalamo-temporal, fronto-striatal, and cerebellar regions, mirroring circuits repeatedly implicated in hallucinations and delusions [31,32]. The same inverse relation appeared for negative symptoms in connections involving the anterior cingulate cortex and precuneus (DMN core),

temporal–sensorimotor pathways, and occipito-parietal links, circuits whose reduced flexibility or hypoconnectivity has been tied to avolition and social withdrawal [33-35]. These observations strengthen the view that limited capacity to reconfigure large-scale networks (high functional inertia) contributes to the clinical phenotype of schizophrenia, in agreement with dynamic-connectivity studies reporting reduced variability within the DMN and fronto-parietal systems [12,18]. Crucially, our results extend that work by showing that whenever these circuits escape inertia, as indexed by cumulative-DTW derivatives, patients report fewer positive and negative symptoms, anchoring the clinical benefit of network flexibility to a directly quantifiable mechanism.

A consistent minority of edges (~17%) showed the opposite pattern: greater FII predicted higher symptom scores. These edges clustered in links that bridge primary sensory or sensorimotor cortices with higher-order association hubs. For positive symptoms, stronger temporal variability between the early visual cortex and the inferior parietal lobule, or between the post-central gyrus and the posterior cingulate cortex, tracked more severe positive symptoms; for negative symptoms, several parieto-occipital couplings showed the same positive relation. Extensive electrophysiological and neuroimaging work indicates that effective sensory integration depends on stable phase synchrony between sensory and association areas, and that excessive volatility degrades perceptual fidelity and contextual gating [36,37]. Dynamic connectivity studies in schizophrenia likewise report reduced variability in default-mode and fronto-parietal systems but heightened fluctuations in sensorimotor, visual, and thalamo-cortical networks [18,38]. Our findings reconcile these prior reports by showing that a rigid high-inertia scaffold can coexist with pockets of hyper-variability, each set of circuits mapping onto symptom severity in distinct ways [12]. This dual motif echoes electrophysiological and computational work suggesting that schizophrenia couples over-stable cortico-cortical hubs to noisy thalamo-sensory loops [19,20]. Consequently, effective interventions may need to loosen pathological rigidity while damping excess volatility, a principle increasingly supported by network-targeted neuromodulation and pharmacotherapy studies [39]. These findings constitute our third cardinal observation: schizophrenia reflects a rigid associative core coupled with a volatile sensory periphery, unified by a common inertial mechanism.

What mechanisms could generate such inertia? Several converging processes can account for the persistence of a configuration in the healthy cortex. Recurrent excitation and slow synaptic integration endow local circuits with short-term “memory,” so that once a pattern is active, it tends to remain active until a strong perturbation intervenes [3]. NMDA-receptor currents, whose decay time constants span hundreds of milliseconds, further stretch the temporal window of integration and bias the network to continue in the same state [40]. At the vascular level, neurovascular coupling unfolds over seconds, so blood flow cannot instantaneously track every neural fluctuation; once a

hemodynamic pattern is established, it resists rapid redistribution and acts as a stabilizing ballast [22,41]. Consistent with this framework, we find that higher inertia in controls correlates with better cognitive performance, suggesting that a moderate resistance filters trivial perturbations while still yielding to meaningful inputs.

In schizophrenia, these normally adaptive mechanisms may become maladaptive. If the ballast is correctly tuned, it promotes stability; if the vessel is already off course, excess ballast impedes correction. Schizophrenia appears to exemplify the latter. Anatomically reinforced loops, such as striato-thalamo-cortical circuits, may create abnormally deep attractor basins that trap activity [39]. Neuroimaging studies consistently show chronic hypofrontality alongside exaggerated sensorimotor drive [42]. Our mediation analysis indicates that prolonged residence in the high-inertia state amplifies symptom severity by reducing global flexibility, implying that an over-rigid functional scaffold cements a dysfunctional pattern (Fig. 4a–d). Yet the opposite abnormality of insufficient inertia may coexist in other circuits. NMDA-receptor hypofunction can shorten synaptic integration windows [43], and dysregulated dopamine can inject excessive variability [44]. This dual disruption aligns with reports of reduced variability in default-mode and fronto-parietal hubs but increased fluctuations in sensorimotor and thalamo-cortical networks [12]. The data suggest that effective interventions must both unlock pathological rigidity in core networks and dampen excess noise in sensory-integration pathways.

From a translational perspective, the cumulative-DTW framework furnishes a single, patient-level index of neural flexibility, capturing how stuck or adaptive the brain is over time. In our cohort, this metric tracked both positive and negative symptom load, suggesting that it could flag individuals with particularly severe dynamic inflexibility and serve as a target for treatment monitoring. Early longitudinal evidence is encouraging: effective antipsychotic therapy increases the diversity of connectivity states and loosens thalamo-cortical constraints, changes that would register as a drop in functional inertia [39]. Network-targeted neuromodulation shows a complementary effect by reducing pathological rigidity in fronto-parietal hubs while damping excess variability in sensory circuits [45]. Cognitive interventions that train flexibility, such as neuroplasticity-based auditory or set-shifting tasks, have likewise been shown to normalize large-scale dynamics and improve outcomes [46]. These observations raise the possibility of precision-medicine strategies that track and ultimately tune the brain's inertial landscape.

Despite these strengths, a methodological limitation warrants note. Our cumulative-window DTW treats the entire history of the BOLD trajectory as equally influential: each new frame is compared with a connectivity profile that aggregates all preceding frames. In vivo, however, neural systems almost certainly weight recent activity more heavily than distant events, with occasional re-entry of older patterns through recurrent loops [1,24]. A recency-weighted or exponentially decaying variant of the algorithm may

therefore capture functional inertia even more faithfully; developing and validating such kernels will be an important next step.

In summary, we demonstrate that large-scale functional networks possess measurable functional inertia and that this temporal property maps onto both healthy cognition and the clinical expression of schizophrenia. Three cardinal observations emerge. First, patients and controls show opposite occupancy of inertia states, with schizophrenia marked by reduced locked-state engagement and greater stabilizing epochs. Second, whole-brain FII not only differentiates groups but mediates how locked-state persistence translates into symptom severity, highlighting its value as a mechanistic biomarker. Third, network-resolved analyses reveal a rigid associative core alongside a volatile sensory periphery, unifying two long-standing observations in schizophrenia under a single inertial framework. By quantifying the resistance each new state must overcome, the cumulative framework offers a novel time-aware lens on whole-brain dynamics. As psychiatry moves toward mechanistic biomarkers, understanding how the brain moves between states may prove as crucial as cataloguing the states themselves. Our work lays the groundwork for that paradigm and points to interventions that both unlock pathological rigidity and temper excessive fluctuation, restoring the balance between stability and flexibility that underpins adaptive cognition.

4. METHODS

4.1. Anchor baseline window

While we introduce a cumulative-window approach to capture network inertia, computing estimates from the first repetition times (TRs) is impractical as early time frames are few, prone to scanner settling artifacts, and yield unreliable estimates. Moreover, because a low-pass filter at $0.01\ Hz$ is applied to BOLD signals, meaningful fluctuations occur over $\sim 100\ s$; more precisely, the $-3dB$ cutoff corresponds to $\sim 88s$ [2,7,47-49]. For these reasons, we define each subject's anchor baseline reference using the first $88s$ of data (after discarding the initial $10\ s$ to allow the scanner's magnetization to reach equilibrium), ensuring enough samples to establish a stable anchor reference. We emphasize that this anchor does not imply comparable "resting tasks" across individuals but rather serves as a common reference against which subsequent frames are evaluated, allowing us to determine whether each new hemodynamic fluctuation reinforces or overcomes that baseline, yielding a more reliable measure of network inertia.

4.2. DTW cumulative window trajectory

Given two post equilibrium BOLD time series $x(t)$ and $y(t)$ of length N, we compute the DTW distance using a Sakoe–Chiba window [15] of half width $w = 88s$, chosen based on the same rationale as the anchor baseline. First, define the local cost:

$$\lambda_\gamma(x_i, y_j) = |x_i - y_j|^\gamma \tag{1}$$

We use $\gamma = 1.5$ as we show in our previous study to be optimal via test-retest reliability and sensitivity to group differences between schizophrenia and controls [17]. The cumulative cost matrix of the DTW algorithm $CM_{(i,j)}$ for $|i - j| \leq w$ is built recursively as:

$$CM_{(i,j)\epsilon\{|i-j|\leq w\}} = \lambda_\gamma(x_i, y_j) + min \begin{cases} CM_{DTW(i-1,j-1)} \\ CM_{DTW(i-1,j)} \\ CM_{DTW(i,j-1)} \end{cases} \tag{2}$$

Once CM is complete, we extract the $\left(\varphi_x(\tau), \varphi_y(\tau)\right)$ of length $|\tau| \geq N$ computed by backtracking from the CM matrix. From this path, the time□resolved DTW distance is defined as:

$$D_{tr}(\tau) = \left|x\left(\varphi_x(\tau)\right) - y\left(\varphi_y(\tau)\right)\right|^{\gamma=1.5} \tag{3}$$

We then apply a piecewise cubic Hermite interpolating polynomial (PCHIP) to $D_{tr}(\tau)$ so that it is resampled at integer time indices $i = 1, \ldots, N$, yielding $D_{tr}^{pchip}(i)$ [17].

Finally, for each $t \geq t_a$, we define the cumulative trajectory as $D_c(t)$, the running average of $D_{tr}^{pchip}(i)$:

$$\underset{t\geq t_a}{D_c(t)} = \frac{1}{t}\sum_{i=1}^{t} D_{tr}^{pchip}(i) \tag{4}$$

4.3. Function inertia index estimation

For each cumulative□window DTW trajectory $c(t)$, we first obtain the smoothed trajectory $\tilde{c}(t)$ using a Gaussian filter, then compute its discrete derivative $\dot{c}(t)$. This derivative represents the FII. Because simple differencing amplifies high□frequency noise, we first apply a Gaussian smoothing whose $-3\ dB$ cutoff matches the point at which the average power spectral density (PSD) of $c(t)$ falls off. Specifically:

I. Compute the mean PSD of $c(t)$ across all subjects. Let f_p be the frequency at which the PSD falls off, indicating where most of the signal power resides.

II. Choose f_p as the Gaussian filter's $-3\ dB$ point (half-power), so that the Gaussian filter has a frequency response as below:

$$|H(f)|^2 = e^{\left[-4(\pi f \sigma_t)^2\right]} = \frac{1}{2} \text{ at } f = f_p$$
$$\sigma_t = \sqrt{\frac{\ln 2}{4\pi^2 f_p^2}} \tag{5}$$

where σ_t is standard deviation of the Gaussian filter (seconds).

III. The time□domain full width at half maximum (FWHM) relates to σ_t by

$$FWHM = 2\sqrt{2\ln 2}\,\sigma_t = 2.3548\sigma_t\ (seconds)$$
$$FWHM = \frac{2.3548\sigma_t}{TR}\ (samples) \tag{6}$$

IV. We therefore apply a Gaussian filter using the derived FWHM to the cumulative metric to get the smoothed cumulative metric $\tilde{c}(t)$.

V. Finally, estimate the discrete derivative via first differences:

$$\dot{c}(t) = \tilde{c}(t) - \tilde{c}(t-1) \tag{7}$$

Using the DTW cumulative-window method with our dataset ($\mathrm{TR} = 2\,s$) yielded a FWHM of 6. This derivative is defined as the **FII**. By construction, higher FII values indicate greater deviation force and thus lower inertia (greater adaptability), whereas values near zero indicate high inertia (rigidity). Gaussian smoothing suppresses high-frequency noise while preserving genuine reconfiguration events, yielding a robust estimate of moment-to-moment functional inertia.

4.4. fMRI data & processing

The We analyzed resting-state fMRI from the Function Biomedical Informatics Research Network (fBIRN) consortium. Data were acquired with a repetition time of 2 s and comprised 160 healthy controls (37.0 ± 10.9 yr, 45 F/115 M) and 151 individuals with schizophrenia (38.8 ± 11.6 yr, 36 F/115 M). Volumes underwent standard preprocessing—slice-timing correction, rigid-body realignment, MNI spatial normalization, and 6 mm FWHM Gaussian smoothing [50]. Spatially independent components were then extracted using the NeuroMark ICA pipeline [51], yielding 53 intrinsic connectivity networks (ICNs) common to all subjects. The resulting ICN time courses were detrended, despiked, and filtered using a Butterworth bandpass filter with a frequency cutoff of $0.01 - 0.15Hz$. The filter, with an optimal order of 7 as determined by MATLAB's *buttord* function, maintained a passband ripple under $3\,dB$ and a minimum stopband attenuation of $30\,dB$. Finally, we standardized the filtered ICNs through z-score transformation.

4.5. Recurrent functional inertia states estimation

fMRI Whole-brain network inertia vectors across brain region pairs were clustered with standard *k*-means because of its widespread use in time-resolved fMRI analysis [12]. We implemented the *k*-means algorithm with cluster numbers ranging from 1 to 10, setting the maximum number of iterations to 10,000 and using 20 random initializations to ensure robust convergence. The city-block (Manhattan) distance metric was selected for its demonstrated robustness in handling high-dimensional data [52]. The optimal cluster number was determined as 3 using the elbow criterion.

4.6. State metrics

Using the *k*-means clusters, we characterized each participant's temporal behavior with three metrics. First, the mean dwell time (MDT) measures state persistence by averaging how long a participant remains in a state once it is entered [53]. Second, the fractional rate (FR) reflects overall occupancy by expressing the proportion of the total recording spent in each state [53]. Finally, the state-to-state transition probabilities form the transition matrix (TM), quantifying how likely a participant is to move from one state to any other [53].

4.7. Group analysis & regression models

We assessed group differences between healthy controls (CN) and individuals with schizophrenia (SZ), associations with the Computerized Multiphasic Interactive Neurocognitive System (CMINDS) cognitive scores, and associations with the Positive and Negative Syndrome Scale (PANSS) symptom score using generalized linear models (GLM) that included age, sex, scanning site, and mean frame displacement (FD) as covariates. For group difference analyses and CMINDS scores, a normal distribution was assumed, whereas a Poisson distribution was applied for PANSS score associations due to the positive integer and skewed and non-negative integer nature of the fBIRN dataset's PANSS scores [17,54]. Multiple comparisons were controlled with the Benjamini–Hochberg false discovery rate (FDR) procedure.

4.8. Global FII & mediation analysis

Because we hypothesize that the brain's overall adaptability may affect clinical and cognitive status, we define the global FII as the average of $|\dot{c}(t)|$ across time, as given below:

$$\frac{1}{N - t_a + 1} \sum_{t=t_a}^{N} |\dot{c}(t)| \tag{8}$$

This summary measure captures the magnitude of deviation force regardless of sign, providing a summary index of overall adaptability (lower global FII indicates higher inertia).

We tested the hypothesis that the influence of a state-level dynamic metric (*X*), such as mean dwell time, on clinical symptom severity (*Y*) is conveyed, in whole or in part, through global FII (*M*). The analytic framework corresponded to a single-mediator model summarized by the causal chain $X \rightarrow M \rightarrow Y$, with adjustment for the same covariates mentioned above (age, sex, FD, and scanner site).

Ordinary least-squares regression was used to estimate:

$$\begin{aligned} \textit{a-path}: &\quad M = \beta_a X + C\gamma_a + \varepsilon_a, \\ \textit{b-and c}'\textit{-paths}: &\quad Y = \beta_b M + B_{c'} X + C\gamma_b + \varepsilon_b, \\ \textit{c-path(total)}: &\quad Y = \beta_c X + C\gamma_c + \varepsilon_c, \end{aligned} \tag{9}$$

$$\textit{indirect effect}: \quad \beta_{indirect} = \beta_a \times \beta_b$$

where X is the predictor (state metric), M is the mediator (global FII), Y is the outcome (symptoms), C is the covariate matrix (age, sex, FD, and site), β are the corresponding coefficients, and ε are the residuals. Statistical significance was evaluated from 5,000 non-parametric bootstrap samples; mediation was deemed significant when the 95% percentile bootstrap confidence interval (CI) excluded zero.

5. ACKNOWLEDGMENT

Sir-Lord Wiafe: Conceptualization, Formal analysis, Methodology, Visualization, Writing –original draft. **Vince Calhoun:** Funding acquisition, Validation, Methodology, Resources, Supervision, Writing – review & editing.

6. FUNDING

This work was supported by the National Institutes of Health (NIH) grant (R01MH123610) and the National Science Foundation (NSF) grant #2112455.

7. DECLARATION OF COMPETING INTEREST

None.

8. DATA & CODE AVAILABILITY STATEMENT

The data was not collected by us and was provided in a deidentified manner. The IRB will not allow sharing of data or individual derivatives as a data reuse agreement was not signed by the subjects during the original acquisition.

9. REFERENCES

1. Murray JD, Bernacchia A, Freedman DJ, et al. A hierarchy of intrinsic timescales across primate cortex. *Nature Neuroscience.* 2014;17(12):1661-1663.
2. Wiafe S-L, Faghiri A, Fu Z, Miller R, Preda A, Calhoun VD. The dynamics of dynamic time warping in fMRI data: a method to capture inter-network stretching and shrinking via warp elasticity. *Imaging Neuroscience.* 2024.
3. Wang XJ. Synaptic reverberation underlying mnemonic persistent activity. *Trends Neurosci.* 2001;24(8):455-463.
4. Major G, Tank D. Persistent neural activity: prevalence and mechanisms. *Curr Opin Neurobiol.* 2004;14(6):675-684.
5. Logothetis NK, Pauls J, Augath M, Trinath T, Oeltermann A. Neurophysiological investigation of the basis of the fMRI signal. *nature.* 2001;412(6843):150-157.
6. Allen EA, Damaraju E, Plis SM, Erhardt EB, Eichele T, Calhoun VD. Tracking whole-brain connectivity dynamics in the resting state. *Cereb Cortex.* 2014;24(3):663-676.
7. Wiafe S-L, Asante NO, Calhoun VD, Faghiri A. Studying time-resolved functional connectivity via communication theory: on the complementary nature of phase synchronization and sliding window Pearson correlation. *bioRxiv.* 2024:2024.2006. 2012.598720.

8. Eickhoff SB, Bzdok D, Laird AR, et al. Co-activation patterns distinguish cortical modules, their connectivity and functional differentiation. *Neuroimage.* 2011;57(3):938-949.
9. Soleimani N, Iraji A, van Erp TGM, Belger A, Calhoun VD. A method for estimating dynamic functional network connectivity gradients (dFNG) from ICA captures smooth inter-network modulation. *bioRxiv.* 2024.
10. Soleimani N, Wiafe S-L, Iraji A, Pearlson G, Calhoun VD. Brain State Convergence and Divergence as Resting State FMRI Biomarkers: A Large-Scale Study of Continuous, Overlapping, Time-resolved States Differentiates Four Psychiatric Disorders. *bioRxiv.* 2025:2025.2005.2020.655164.
11. Gaviria J, Rey G, Bolton T, Ville DVD, Vuilleumier P. Dynamic functional brain networks underlying the temporal inertia of negative emotions. *NeuroImage.* 2021;240:118377.
12. Damaraju E, Allen EA, Belger A, et al. Dynamic functional connectivity analysis reveals transient states of dysconnectivity in schizophrenia. *NeuroImage: Clinical.* 2014;5:298-308.
13. Rashid B, Damaraju E, Pearlson GD, Calhoun VD. Dynamic connectivity states estimated from resting fMRI Identify differences among Schizophrenia, bipolar disorder, and healthy control subjects. *Front Hum Neurosci.* 2014;8:897.
14. Rolls ET, Loh M, Deco G, Winterer G. Computational models of schizophrenia and dopamine modulation in the prefrontal cortex. *Nature Reviews Neuroscience.* 2008;9(9):696-709.
15. Paliwal KK, Agarwal A, Sinha SS. A modification over Sakoe and Chiba's dynamic time warping algorithm for isolated word recognition. *Signal Processing.* 1982;4(4):329-333.
16. Wiafe S-L, Kinsey S, Iraji A, Miller R, Calhoun VD. Normalized Dynamic Time Warping Increases Sensitivity In Differentiating Functional Network Connectivity In Schizophrenia. *bioRxiv.* 2024:2024.2010.2031.621415.
17. Wiafe S-L, Kinsey S, Soleimani N, et al. Mapping Dynamic Metabolic Energy Distribution in Brain Networks using fMRI: A Novel Dynamic Time Warping Framework. *bioRxiv.* 2025:2025.2003. 2020.644399.
18. You W, Luo L, Yao L, et al. Impaired dynamic functional brain properties and their relationship to symptoms in never treated first-episode patients with schizophrenia. *Schizophrenia.* 2022;8(1):90.
19. Uhlhaas PJ, Singer W. Abnormal neural oscillations and synchrony in schizophrenia. *Nature Reviews Neuroscience.* 2010;11(2):100-113.
20. Rolls ET, Deco G. A computational neuroscience approach to schizophrenia and its onset. *Neurosci Biobehav Rev.* 2011;35(8):1644-1653.
21. Attwell D, Laughlin SB. An energy budget for signaling in the grey matter of the brain. *Journal of Cerebral Blood Flow & Metabolism.* 2001;21(10):1133-1145.
22. Magistretti Pierre J, Allaman I. A Cellular Perspective on Brain Energy Metabolism and Functional Imaging. *Neuron.* 2015;86(4):883-901.
23. Raichle ME, Mintun MA. Brain work and brain imaging. *Annu Rev Neurosci.* 2006;29:449-476.
24. Vidaurre D, Smith SM, Woolrich MW. Brain network dynamics are hierarchically organized in time. *Proceedings of the National Academy of Sciences.* 2017;114(48):12827-12832.
25. Mitra A, Snyder AZ, Hacker CD, Raichle ME. Lag structure in resting-state fMRI. *J Neurophysiol.* 2014;111(11):2374-2391.
26. Dwyer DS, Bradley RJ, Kablinger AS, Freeman AM, 3rd. Glucose metabolism in relation to schizophrenia and antipsychotic drug treatment. *Ann Clin Psychiatry.* 2001;13(2):103-113.
27. Newcomer JW, Haupt DW, Fucetola R, et al. Abnormalities in glucose regulation during antipsychotic treatment of schizophrenia. *Arch Gen Psychiatry.* 2002;59(4):337-345.
28. Li CS. Do schizophrenia patients make more perseverative than non-perseverative errors on the Wisconsin Card Sorting Test? A meta-analytic study. *Psychiatry Res.* 2004;129(2):179-190.

29. Duan X, Hu M, Huang X, et al. Effect of Risperidone Monotherapy on Dynamic Functional Connectivity of Insular Subdivisions in Treatment-Naive, First-Episode Schizophrenia. *Schizophr Bull.* 2020;46(3):650-660.
30. Corriveau A, Yoo K, Kwon YH, Chun MM, Rosenberg MD. Functional connectome stability and optimality are markers of cognitive performance. *Cereb Cortex.* 2023;33(8):5025-5041.
31. Forlim CG, Klock L, Gallinat J, Kühn S. Altered resting-state functional connectivity in a thalamo-cortico-cerebellar network in patients with schizophrenia. *Sci Rep.* 2024;14(1):26284.
32. Bernard JA, Orr JM, Mittal VA. Cerebello-thalamo-cortical networks predict positive symptom progression in individuals at ultra-high risk for psychosis. *Neuroimage Clin.* 2017;14:622-628.
33. Opjordsmoen S. Delusional Disorder as a Partial Psychosis. *Schizophrenia Bulletin.* 2014;40(2):244-247.
34. Manoliu A, Riedl V, Doll A, et al. Insular Dysfunction Reflects Altered Between-Network Connectivity and Severity of Negative Symptoms in Schizophrenia during Psychotic Remission. *Frontiers in Human Neuroscience.* 2013;Volume 7 - 2013.
35. Moessnang C, Otto K, Bilek E, et al. Differential responses of the dorsomedial prefrontal cortex and right posterior superior temporal sulcus to spontaneous mentalizing. *Hum Brain Mapp.* 2017;38(8):3791-3803.
36. Zhou G, Lane G, Noto T, et al. Human olfactory-auditory integration requires phase synchrony between sensory cortices. *Nature Communications.* 2019;10(1):1168.
37. Varela F, Lachaux J-P, Rodriguez E, Martinerie J. The brainweb: Phase synchronization and large-scale integration. *Nature Reviews Neuroscience.* 2001;2(4):229-239.
38. Dong D, Duan M, Wang Y, et al. Reconfiguration of Dynamic Functional Connectivity in Sensory and Perceptual System in Schizophrenia. *Cerebral Cortex.* 2018;29(8):3577-3589.
39. Yang M, Liu L, Cui H, et al. Dynamic functional thalamocortical dysconnectivity in schizophrenia correlates to antipsychotics response. *Schizophrenia.* 2023;9(1):40.
40. Wang X-J. Synaptic Basis of Cortical Persistent Activity: the Importance of NMDA Receptors to Working Memory. *The Journal of Neuroscience.* 1999;19(21):9587-9603.
41. Logothetis NK. What we can do and what we cannot do with fMRI. *Nature.* 2008;453(7197):869-878.
42. Minzenberg MJ, Laird AR, Thelen S, Carter CS, Glahn DC. Meta-analysis of 41 Functional Neuroimaging Studies of Executive Function in Schizophrenia. *Archives of General Psychiatry.* 2009;66(8):811-822.
43. Balu DT. The NMDA Receptor and Schizophrenia: From Pathophysiology to Treatment. *Adv Pharmacol.* 2016;76:351-382.
44. Winterer G, Weinberger DR. Cortical signal-to-noise ratio: insight into the pathophysiology and genetics of schizophrenia. *Clinical Neuroscience Research.* 2003;3(1):55-66.
45. Csukly G, Orbán-Szigeti B, Suri K, et al. Theta-burst rTMS in schizophrenia to ameliorate negative and cognitive symptoms: study protocol for a double-blind, sham-controlled, randomized clinical trial. *Trials.* 2024;25(1):269.
46. Fisher M, Holland C, Merzenich MM, Vinogradov S. Using neuroplasticity-based auditory training to improve verbal memory in schizophrenia. *Am J Psychiatry.* 2009;166(7):805-811.
47. Faghiri A, Iraji A, Damaraju E, Turner J, Calhoun VD. A unified approach for characterizing static/dynamic connectivity frequency profiles using filter banks. *Network Neuroscience.* 2021;5(1):56-82.
48. Faghiri A, Yang K, Ishizuka K, Sawa A, Adali T, Calhoun V. *Frequency modulation increases the specificity of time-resolved connectivity: A resting-state fMRI study.* 2023.
49. Wiafe S-L, Faghiri A, Fu Z, Miller R, Calhoun V. *Capturing Stretching and Shrinking of Inter-Network Temporal Coupling in FMRI Via WARP Elasticity.* 2024.

50. Penny WD, Friston KJ, Ashburner JT, Kiebel SJ, Nichols TE. *Statistical parametric mapping: the analysis of functional brain images.* Elsevier; 2011.
51. Du Y, Fu Z, Sui J, et al. NeuroMark: An automated and adaptive ICA based pipeline to identify reproducible fMRI markers of brain disorders. *Neuroimage Clin.* 2020;28:102375.
52. Aggarwal CC, Hinneburg A, Keim DA. On the surprising behavior of distance metrics in high dimensional space. Paper presented at: Database Theory—ICDT 2001: 8th International Conference London, UK, January 4–6, 2001 Proceedings 82001.
53. Iraji A, Faghiri A, Lewis N, Fu Z, Rachakonda S, Calhoun VD. Tools of the trade: estimating time-varying connectivity patterns from fMRI data. *Social Cognitive and Affective Neuroscience.* 2020;16(8):849-874.
54. Santoro ML, Ota V, de Jong S, et al. Polygenic risk score analyses of symptoms and treatment response in an antipsychotic-naive first episode of psychosis cohort. *Transl Psychiatry.* 2018;8(1):174.